

## Large-scale dynamics of magnetic helicity

Moritz Linkmann<sup>1,2,\*</sup> and Vassilios Dallas<sup>3,†</sup>

<sup>1</sup>*Department of Physics and INFN, University of Rome Tor Vergata,  
Via della Ricerca Scientifica 1, 00133 Rome, Italy*

<sup>2</sup>*SUPA, School of Physics and Astronomy, University of Edinburgh, Peter Guthrie Tait Road, EH9 3FD, UK*

<sup>3</sup>*Department of Applied Mathematics, University of Leeds, Leeds LS2 9JT, UK*

In this paper we investigate the dynamics of magnetic helicity in magnetohydrodynamic (MHD) turbulent flows focusing at scales larger than the forcing scale. Our results show a nonlocal inverse cascade of magnetic helicity, which occurs directly from the forcing scale into the largest scales of the magnetic field. We also observe that no magnetic helicity and no energy is transferred to an intermediate range of scales sufficiently smaller than the container size and larger than the forcing scale. Thus, the statistical properties of this range of scales, which increases with scale separation, is shown to be described to a large extent by the zero flux solutions of the absolute statistical equilibrium theory exhibited by the truncated ideal MHD equations.

The current explanation for the existence of stellar and planetary magnetic fields is attributed to dynamo action [1]. One of the theoretical arguments to explain the generation and preservation of magnetic fields in spatial scales much larger than the outer scales of fluid motions is the inverse cascade of magnetic helicity in MHD turbulence [2]. Magnetic helicity plays a fundamental role in the long-term evolution of stellar and planetary magnetic fields [3] and hence its dynamics across scales is important to shed light on the saturation mechanisms of these large-scale magnetic fields.

Previous investigations concerning the inverse cascade of magnetic helicity reported both local and nonlocal transfers with various scaling exponents measured for the spectra at large scales [4–6]. However, it is presently unclear whether these local and non-local transfers should be associated with a process that takes place with constant flux [7]. Due to growing evidence for the importance of non-local interactions in the dynamics of MHD turbulence [4, 7–9], concern has been raised over the use of the term *cascade* [6, 10]. Therefore, in our context the term *cascade* does not necessarily imply locality in wavenumber space.

In spite of the importance of the inverse cascade of magnetic helicity, there is a lack of understanding about its non-linear dynamics at large scales. In this paper we aim to elucidate the steady-state dynamics of magnetic helicity and its role in the long time evolution of the large-scale magnetic field. To do this we consider flows with high enough scale separation by applying helical electromagnetic forcing at intermediate scales using direct numerical simulations (DNS) and we focus on the dynamical and statistical properties of the large scales. We show that the inverse cascade of magnetic helicity is a manifestation of non-local transfers from the forcing scale

to the largest scales of the magnetic field in agreement with previous studies [4, 5]. Moreover, we demonstrate that despite the fact that in three-dimensional MHD turbulence the scales between the forcing scale and the container size are not isolated from the turbulent scales, their statistics may still be reasonably approximated as if they were in statistical equilibrium for high enough scale separation.

In planets and stars as well as in laboratory experiments, physical boundaries confine fluids and set the largest possible characteristic length scale of the flow. In our DNS, the size of the periodic box  $2\pi L$  is the surrogate for this spatial confinement. In order to study the large-scale dynamics of turbulence, large enough scale separation is necessary between the box size and the forcing scale, while at the same time one has to ensure that small-scale turbulence is still resolved. Forcing at intermediate scales and aiming for a turbulent flow with high enough scale separation is therefore almost prohibitive even with today's supercomputers. We partly circumvent this difficulty by considering hyper-dissipative terms under the assumption that the dissipative scales should not significantly affect the statistical properties of the large scales. Due to the presence of the inverse cascade of magnetic helicity we consider a large-scale dissipation mechanism to saturate the expected energy growth. Otherwise, energy accumulates in the largest scales of the box until it is balanced by viscosity leading to the formation of very large amplitude vortices [11]. Therefore, we consider the following dynamical equations:

$$\begin{aligned} (\partial_t - \nu^- \Delta^{-m} - \nu^+ \Delta^n) \mathbf{u} &= \mathbf{u} \times \boldsymbol{\omega} + \mathbf{j} \times \mathbf{b} - \nabla P + \mathbf{f}_u, \\ (\partial_t - \eta^- \Delta^{-m} - \eta^+ \Delta^n) \mathbf{b} &= \nabla \times (\mathbf{u} \times \mathbf{b}) + \mathbf{f}_b, \end{aligned} \quad (1)$$

where  $\mathbf{u}$  denotes the velocity field,  $\mathbf{b}$  the magnetic induction expressed in Alfvén units,  $\boldsymbol{\omega} = \nabla \times \mathbf{u}$  the vorticity,  $\mathbf{j} = \nabla \times \mathbf{b}$  the current density,  $P$  the pressure,  $\mathbf{f}_u$  and  $\mathbf{f}_b$  the external mechanical and electromagnetic forces, respectively. Energy is dissipated at the small scales by the terms proportional to  $\nu^+$  and  $\eta^+$  and at the large

\* linkmann@roma2.infn.it

† v.dallas@leeds.ac.uk

scales by  $\nu^-$  and  $\eta^-$ . The indices  $n, m$  specify the order of the Laplacian used. In order to obtain a large inertial range, we chose  $n = m = 4$ . For all runs, we chose  $\nu^+ = \eta^+$  and  $\nu^- = \eta^-$ . In the absence of forcing and dissipation, Eqs. (1) reduce to the ideal MHD equations, which have three conserved quantities: the total energy  $E = E_u + E_b = \frac{1}{2} \sum_{\mathbf{k}} (|\mathbf{u}_{\mathbf{k}}|^2 + |\mathbf{b}_{\mathbf{k}}|^2)$ , the magnetic helicity  $H_b = \sum_{\mathbf{k}} \mathbf{a}_{\mathbf{k}} \cdot \mathbf{b}_{-\mathbf{k}}$ , and the cross-helicity  $H_c = \sum_{\mathbf{k}} \mathbf{u}_{\mathbf{k}} \cdot \mathbf{b}_{-\mathbf{k}}$ , where  $\mathbf{a}$  denotes the vector potential of the magnetic field.

The forces  $\mathbf{f}_u$  and  $\mathbf{f}_b$  are constructed from a randomized superposition of eigenfunctions of the curl operator [4, 6, 12], resulting in Gaussian distributed and  $\delta(t)$ -correlated forces whose helicities  $\langle \mathbf{f}_{u,b} \cdot \nabla \times \mathbf{f}_{u,b} \rangle$  and correlation  $\langle \mathbf{f}_u \cdot \mathbf{f}_b \rangle$  can be exactly controlled ( $\langle \cdot \rangle$  indicates spatial averages unless indicated otherwise). The specific random nature of the forces ensures that at steady state the total energy input rate  $\varepsilon = \varepsilon_u + \varepsilon_b = \langle \mathbf{u} \cdot \mathbf{f}_u \rangle + \langle \mathbf{b} \cdot \mathbf{f}_b \rangle \propto |\mathbf{f}_u|^2 + |\mathbf{f}_b|^2$  is known *a priori* [13] with  $|\mathbf{f}_u| = |\mathbf{f}_b| = f_0$ . In this case,  $\varepsilon$  can be used as a control parameter. Note that we choose to force both  $\mathbf{u}$  and  $\mathbf{b}$  with the same forcing amplitude so that both quantities are dynamically important and  $\mathbf{b}$  has a nonlinear feedback on the flow through the Lorenz force.

The use of an electromagnetic forcing is typical in studies that have focused on the dynamics of magnetic helicity [5, 6, 12] in contrast to dynamo studies. Realistic analogues of such a forcing are, for example, the toroidal current that is driven in tokamaks in order to generate a poloidal magnetic field, and the force that is applied in electromagnetic pumps, which are driven by means of a traveling magnetic field imposed by external coils. Note that our intention in this study is not to simulate such a system but to further understand the dynamics of  $H_b$ , whose interpretation from dynamo simulations is ambiguous because in these simulations  $H_b$ , and most importantly its mean flux, change sign in the inertial range of scales. However, by forcing the induction equation it is possible to maintain a sign-definite mean value of  $H_b$ , which allows us to study the non-linear dynamics of magnetic helicity across scales unambiguously.

The forces are chosen such that the helicity of  $\mathbf{f}_u$  is negligible while  $\mathbf{f}_b$  is fully helical for all simulations; and they are decorrelated, i.e.,  $\langle \mathbf{f}_u \cdot \mathbf{f}_b \rangle = 0$ . Thus, no  $H_c$  and no kinetic helicity  $H_u = \langle \mathbf{u} \cdot \boldsymbol{\omega} \rangle$  are injected into the flow, while the injection of  $H_b$  is maximal. Here, we exclude the injection of cross-helicity in the flow in order to avoid introducing correlations between the velocity and the magnetic field which would affect the cascade dynamics of the conserved quantities [10]. Moreover, we avoid injecting kinetic helicity into the flow in order to exclude any generation of mean magnetic helicity due to the presence of a strong component of mean kinetic helicity in the flow. Finally, the initial Gaussian distributed random magnetic and velocity fields are in equipartition with energy spectra peaked at the forcing wave number  $k_f$  and zero helicities, i.e.,  $H_b = H_c = H_u = 0$ . We should point out here that  $H_c$  remains negligible in our flows, however,

$k_f L$	$N$	$Re_f$	$\nu^+ = \eta^+$	$\nu^- = \eta^-$	$f_0$	$T/t_f$
10	128	$7 \times 10^3$	$6.30 \times 10^{-12}$	0.05	1	320
20	256	$7 \times 10^3$	$4.92 \times 10^{-14}$	0.05	$\sqrt{2}$	130
40	512	$7 \times 10^3$	$3.68 \times 10^{-16}$	0.05	2	100

TABLE I. Numerical parameters of the simulations. Note that  $k_f$  denotes the forcing wavenumber,  $T$  the total runtime in simulation units,  $f_0 = |\mathbf{f}_u| = |\mathbf{f}_b|$  the forcing amplitude and  $t_f \equiv (u_f k_{box})^{-1}$  a timescale defined based on the control parameters. All simulations are well resolved with  $k_{cut}/k_d \geq 1.25$ .

$H_u$  increases with  $H_u / (\langle |\mathbf{u}|^2 \rangle \langle |\boldsymbol{\omega}|^2 \rangle)^{1/2} \simeq 0.2$  at steady state.

Equations (1) are solved numerically using the standard pseudospectral method, which ensures that  $\nabla \cdot \mathbf{u} = 0$  and  $\nabla \cdot \mathbf{b} = 0$ . Full dealiasing is achieved by the 2/3-rule and as a result the minimum and maximum wave numbers are  $k_{box} = 1$  and  $k_{cut} = N/3$ , respectively, where  $N$  is the number of grid points in each Cartesian coordinate. Further details of the code can be found in Refs. [14, 15].

Following previous studies [16, 17], a Reynolds number may be defined based on the control parameters of the problem as  $Re_f \equiv u_f k_f^{1-2n} / \nu^+$  with  $u_f \equiv (\varepsilon / k_f)^{1/3}$ . In the following,  $\varepsilon$  and  $\nu^+$  are adjusted such that  $u_f$ , and the ratio of  $k_{cut}$  with the dissipation wave number  $k_d \equiv (\varepsilon / (\nu^+)^3)^{1/(6n-2)}$  remain the same for the different simulations. That is,  $\varepsilon / k_f$  is kept constant between simulations while increasing the scale separation  $k_f L$ . This results in the same Reynolds number, which highlights that the only difference between the simulations is the scale separation between  $k_f$  and  $L$ . The numerical parameters of the simulations are given in Table I.

The flux of total energy  $\Pi_E(k)$  and magnetic helicity  $\Pi_{H_b}(k)$  in Fourier space is given by

$$\begin{aligned} \Pi_E(k) &\equiv \langle \mathbf{u}_{\mathbf{k}}^< (\mathbf{u} \cdot \nabla \mathbf{u} - \mathbf{b} \cdot \nabla \mathbf{b}) \rangle + \langle \mathbf{b}_{\mathbf{k}}^< (\mathbf{u} \cdot \nabla \mathbf{b} - \mathbf{b} \cdot \nabla \mathbf{u}) \rangle, \\ \Pi_{H_b}(k) &\equiv \langle \mathbf{a}_{\mathbf{k}}^< (\mathbf{b} \cdot \nabla \mathbf{u} - \mathbf{u} \cdot \nabla \mathbf{b}) \rangle, \end{aligned} \quad (2)$$

where the notation  $g_{\mathbf{k}}^<$  denotes the Fourier filtered field  $g$  such that only the modes satisfying  $|\mathbf{k}| \leq k$  are kept [18]. Negative values of the fluxes imply inverse cascades while positive values imply forward cascades.

The strength of forward and inverse cascades of a conserved quantity at steady state can be quantified by the rate of dissipation in the small and large scales, respectively, which we define as  $\varepsilon^\pm \equiv 2\nu^\pm \left\langle \sum_{\mathbf{k} \neq 0} k^{\pm 2n} (|\mathbf{u}_{\mathbf{k}}|^2 + |\mathbf{b}_{\mathbf{k}}|^2) \right\rangle$ , where  $\langle \cdot \rangle$  denotes a time-average in this case. Then, the total energy dissipation rate is given by  $\varepsilon = \varepsilon^+ + \varepsilon^-$ . A similar decomposition can be made for the dissipation rate of  $H_b$  resulting in  $\varepsilon_{H_b} = \varepsilon_{H_b}^- + \varepsilon_{H_b}^+$  with  $\varepsilon_{H_b}^\pm \equiv 2\nu^\pm \left\langle \sum_{\mathbf{k} \neq 0} k^{\pm 2n} (\mathbf{a}_{\mathbf{k}} \cdot \mathbf{b}_{-\mathbf{k}}) \right\rangle$ .

Since we are interested in the behavior of the total energy and the magnetic helicity at large scales we need to ensure that our simulations have been integrated for long

enough times so that the largest scales are in a statistically stationary state. This is satisfied when  $\varepsilon^-$  reaches a saturated state. In what follows we analyze the data from these saturated states.

Absolute equilibrium (zero-flux) statistical mechanics have been used effectively to suggest the directions of cascades (finite flux) of the ideal conserved quantities across scales. In particular, it has been shown [2] that energy is transferred toward small scales (forward cascade) while magnetic helicity is transferred toward large scales (inverse cascade). In order to check if these predictions are true in our flows we plot  $\Pi_E(k)$  and  $\Pi_{H_b}(k)$  normalized by their dissipation rates (see Fig. 1). The

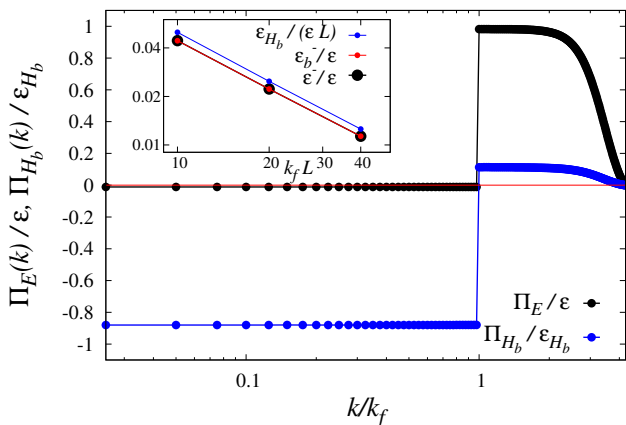


FIG. 1. Fluxes of total energy and magnetic helicity normalized with the corresponding dissipation rates for the run with  $k_f L = 40$ . Black: normalized total energy flux  $\Pi_E(k)/\varepsilon$ . Blue (dark gray): normalized magnetic helicity flux  $\Pi_{H_b}(k)/\varepsilon_{H_b}$ . The inset presents the scaling  $\varepsilon^-/\varepsilon \propto \varepsilon_{H_b}/(\varepsilon L) \propto (k_f L)^{-1}$ . Black:  $\varepsilon^-/\varepsilon$ . Red (light gray):  $\varepsilon_b^-/\varepsilon$ . Blue (dark gray):  $\varepsilon_{H_b}/(\varepsilon L)$ .

total energy has a forward cascade with  $\Pi_E(k) > 0$  for  $k \geq k_f$ , while  $\Pi_E(k) \simeq 0$  for  $k < k_f$ . The magnetic helicity, however, has a dual cascade toward large and small scales, even though the injection of  $H_b$  is maximal, with  $\sim 90\%$  of  $\Pi_{H_b}(k)$  being negative (i.e.,  $\varepsilon_{H_b}^- \simeq 0.9\varepsilon_{H_b}$ ) at  $k < k_f$ . From the inset of Fig. 1, we observe that  $\varepsilon^- = \varepsilon_b^- \propto \varepsilon_{H_b}/L \propto (k_f L)^{-1}\varepsilon$ . This scaling implies that the ratio  $\varepsilon_{H_b}/(\varepsilon L)$  determines the fraction of the total energy flux that proceeds toward large scales. This can be partly understood from the relation between the injection rates of  $H_b$  and  $E_b$  due to the helical  $\mathbf{f}_b$  forcing, i.e.,

$$\varepsilon_{H_b} = \langle \mathbf{a} \cdot \mathbf{f}_b \rangle = k_f^{-1} \langle \mathbf{a} \cdot (\nabla \times \mathbf{f}_b) \rangle = k_f^{-1} \langle \mathbf{b} \cdot \mathbf{f}_b \rangle = k_f^{-1} \varepsilon_b. \quad (3)$$

Note that no matter how  $\varepsilon_b$  (and therefore  $\varepsilon$ ) may be varied with  $k_f$ , one obtains  $\varepsilon_b^-/\varepsilon \propto (k_f L)^{-1}$ , that is, for  $k_f L \gg 1$  we expect  $\Pi_{E_b}(k) = \varepsilon_b^- \rightarrow 0$  at  $k < k_f$  and hence  $\Pi_E(k) = \varepsilon^- \rightarrow 0$  at  $k < k_f$  since  $\varepsilon^- = \varepsilon_b^-$  (see the inset of Fig. 1). In other words, the inverse flux of total energy will become negligible once the separation

between the forcing scale and the largest scale of the system becomes very large. This results in a weak energy input to sustain large-scale magnetic fields.

According to Fig. 1,  $H_b$  has a constant negative flux at  $k < k_f$ , which implies an inverse cascade. This is based on the idea that the time-averaged transfer is zero in some intermediate wave-number range for flows with large enough scale separation [19]. We should point out here that zero time-averaged transfer does not necessarily mean constant nonzero  $H_b$  transfer (i.e., no gain or loss of  $H_b$  in a particular wave number  $k$ ), it can also mean zero  $H_b$  transfer between modes. Considering the instantaneous transfers,

$$T_{H_b}(k, t) \equiv \sum_{|\mathbf{k}|=k} \sum_{\mathbf{p}+\mathbf{q}=\mathbf{k}} \mathbf{b}_{-\mathbf{k}} \cdot (\mathbf{u}_{\mathbf{p}} \times \mathbf{b}_{\mathbf{q}}), \quad (4)$$

at steady state (see Fig. 2), we see that  $T_{H_b}(k, t) = 0$  for  $5 < k < k_f$ , implying not only vanishing average transfer but also no instantaneous transfer of  $H_b$  into the large scales, apart from the fluctuations that are observed at the low  $k$  modes. Therefore, this observation suggests a nonlocal transfer of magnetic helicity from the forcing scale to the largest scales of the magnetic field.

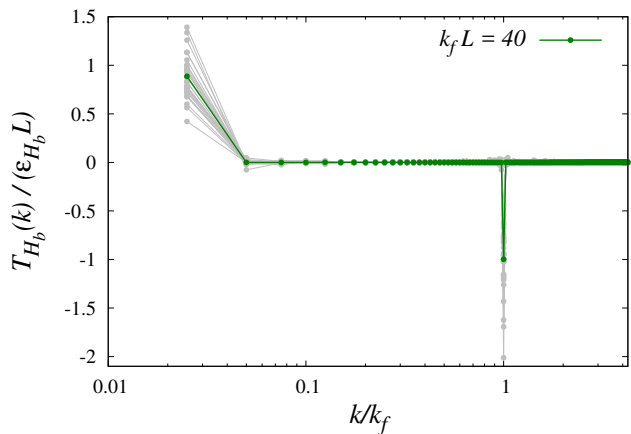


FIG. 2. Transfer spectra of magnetic helicity normalized with  $\varepsilon_{H_b} L$  for the flow with  $k_f L = 40$ . The time-averaged transfer  $T_{H_b}(k)$  is indicated by the green (dark gray) curve while the gray curves indicate the instantaneous transfers  $T_{H_b}(k, t)$ .

To be precise on this statement, we analyze the shell-to-shell transfers [5, 7] of magnetic helicity,

$$T_{H_b}(K, Q) \equiv \int \mathbf{b}_K \cdot (\mathbf{u} \times \mathbf{b}_Q) d^3 \mathbf{x} \quad (5)$$

from shell  $Q$  to shell  $K$ . This transfer term conserves magnetic helicity, that is, it does not generate or destroy  $H_b$ , but it is responsible for the redistribution of  $H_b$  across different scales. This is expressed by the fact that  $T_{H_b}(K, Q)$  is antisymmetric under the exchange of  $K$  and  $Q$ , i.e.,  $T_{H_b}(K, Q) = -T_{H_b}(Q, K)$ , which is confirmed by Fig. 3.

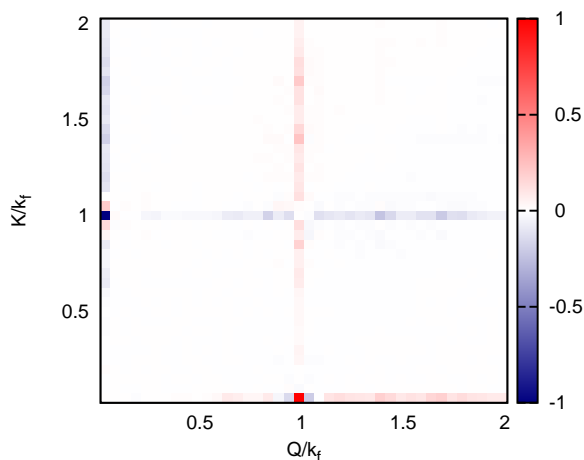


FIG. 3. Instantaneous normalized magnetic helicity transfer  $T_{H_b}(K, Q)/(\epsilon_{H_b} L)$  from shell  $Q$  to shell  $K$  rescaled with  $k_f$ .

Figure 3 shows that all transfers of  $H_b$  between wave numbers smaller than  $k_f$  vanish apart from the transfer from the forced shell  $Q/k_f = 1$  to the smallest shell  $K/k_f$ . Therefore, the Fourier modes at  $k_f$  interact nonlocally with the Fourier modes at  $k = 1$  while the intermediate wave numbers  $1 < k < k_f$  have  $T_{H_b}(K, Q) = 0$  and hence  $\Pi_{H_b}(k) = 0$  in this range. In other words, the constant negative value of  $\Pi_{H_b}(k)$  in the  $k < k_f$  regime is a manifestation of nonlocal transfers of  $H_b$  from the forcing scale to the largest scale of the magnetic field.

In summary, as we increase  $k_f L$  we observe  $\Pi_E(k) \rightarrow 0$  at  $k < k_f$  and  $\Pi_{H_b}(k) = 0$  at  $5 < k < k_f$ . Therefore, we expect the large-scale flow to be described to a large extent from the predictions of the zero-flux solutions given by absolute equilibrium statistical mechanics [18, 20]. To verify this we examine the scaling of our spectra at scales larger than the forcing length scale but also sufficiently smaller than the box size and we compare with the predictions from absolute equilibrium theory, which we present below.

Following Ref. [2], we consider the Boltzmann-Gibbs distribution for the truncated ideal 3D MHD equations (i.e., only Fourier modes  $k_{min} \leq k \leq k_{max}$  are kept,  $k_{max}$  being the truncation wave number) with zero cross-helicity,  $\mathcal{P} = Z^{-1} \exp(-\alpha E - \beta H_b)$ , where  $Z$  is the partition function of a Gaussian ensemble. The coefficients  $\alpha$  and  $\beta$  are determined by the total energy and the magnetic helicity of the system and can be interpreted as the inverse temperatures in the classical thermodynamic equilibrium sense. Using the discrete form of  $E$  and  $H_b$  we can obtain the following expressions for their spectral

densities at absolute equilibrium:

$$\begin{aligned} E_u(k) &= \frac{4\pi}{\alpha} k^2, \\ E_b(k) &= \frac{4\pi}{\alpha} \frac{k^2}{1 - (\frac{\beta}{\alpha k})^2}, \\ H_b(k) &= -\frac{4\pi\beta}{\alpha^2} \frac{1}{1 - (\frac{\beta}{\alpha k})^2}. \end{aligned} \quad (6)$$

In order for  $\mathcal{P}$  to be normalizable, i.e., the quadratic form  $\alpha E + \beta H_b$  to be positive definite, we need  $\alpha > 0$  and  $\alpha > |\beta|/k_{min}$ . These spectra have a singularity at wavenumber  $k_s \equiv |\beta|/\alpha < k_{min}$  outside the validity of Eqs. (6).

Equations (6) suggest equipartition of kinetic energy across scales while magnetic energy equipartition is only true for  $k \gg k_s$ . As  $k \rightarrow k_{min}$  the values of  $E_b(k)$  and  $H_b(k)$  diverge for values of  $k_s$  close to  $k_{min}$ . The region near  $k_{min}$  has maximal helicity where the total energy  $E$  is dominated by  $E_b$  and therefore  $k_{min}|H_b| \simeq E$ . This divergence of  $H_b(k)$  at low  $k$  (which is a conserved quantity unlike  $E_b$ ) is the indicator of the corresponding magnetic helicity transfer toward large scales.

Figure 4(a) shows the magnetic and kinetic energy spectra compensated with  $k^{-2}$ , with the  $E_u$  spectra being shifted by a factor of  $10^{-3}$  for clarity. Note that  $E_u(k)/E_b(k) \sim 1$  for wave numbers  $k/k_f \geq 0.3$ . The spectra here collapse by rescaling with  $k/k_f$ . Our data displays the scaling  $E_u(k) \propto k^2$  at low wavenumbers  $k < k_f$  with the range of validity increasing with  $k_f L$ . The magnetic energy spectra show a  $E_b(k) \propto k^2$  scaling while the magnetic helicity [see Fig. 4(b)] show  $H_b(k) \propto k^0$  for an intermediate range of wavenumbers  $k_{box} \ll k < k_f$ . These scalings are in agreement with the predictions of the absolute equilibria for the truncated ideal MHD equations. We point out that altering the hypodiffusive exponent  $m$  does not affect the scaling of the spectra at the large scales.

In order to compare the numerical results with the predictions of the absolute equilibrium theory, we have plotted Eqs. (6) as dashed lines in Fig. 4 using values of  $\alpha$  and  $\beta$  obtained from a linear fit. A measurable deviation from the theory is observed as  $k \rightarrow k_{box}$ . The amplitude of the deviation is independent of the dissipation mechanism and only weakly dependent on scale separation. The dashed lines in Fig. 4 predict that the divergence of the spectra at  $k_s = |\beta|/\alpha$  is expected at  $k_s/k_f = 3.5 \cdot 10^{-4}$ , which is beyond the expected validity of the absolute equilibrium regime. Therefore, the deviations from the power-law scalings are due to other possible reasons. The most important reason affecting the magnetic energy spectra is the minimal but still finite negative flux of  $E_b$  at large scales. However, we expect better agreement of  $E_b(k)$  with the corresponding absolute equilibrium prediction as scale separation increases because  $\epsilon_b^-/\epsilon \propto (k_f L)^{-1}$ . The nonlocal transfers of magnetic helicity from the forcing scale to the largest scales ( $1 \leq k \leq 5$ ) of the flow is an obvious reason for  $H_b(k)$

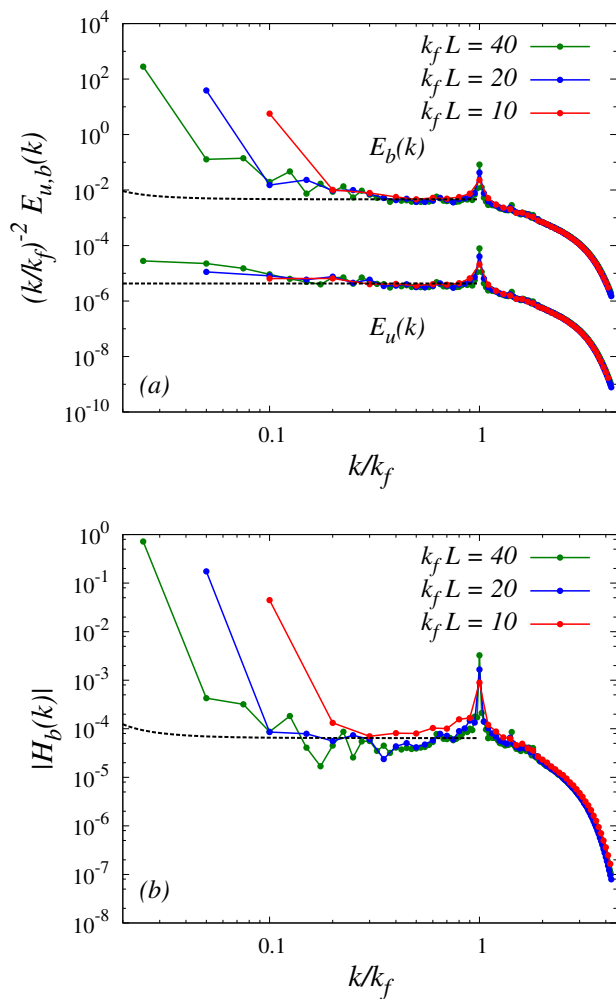


FIG. 4. (a) Magnetic and kinetic energy spectra compensated by  $k^{-2}$ , where  $E_u(k)$  has been shifted by a factor of  $10^{-3}$ . (b) Absolute value of magnetic helicity spectra. The spectra are collapsed by rescaling with  $k/k_f$ . The dashed lines correspond to the predictions from absolute equilibria, i.e. Eqs. (6). The green (light gray) curves refers to the simulation with  $k_f L = 40$ , the blue (dark gray) to  $k_f L = 20$  and the red (gray) to  $k_f L = 10$ . The inset shows the absolute value of the relative magnetic helicity  $\rho_b(k) = H_b(k)/(\langle |\mathbf{a}_k|^2 \rangle^{1/2} \langle |\mathbf{b}_k|^2 \rangle^{1/2})$

to disagree with the equilibrium predictions. Finally, for wave numbers close to  $k_{box}$  the assumptions of isotropy used in the derivation of Eqs. (6) are not valid and deviations from the isotropic result are expected for all the

spectra in Fig. 4.

In the inset of Fig. 4(b), we also plot the absolute value of the relative magnetic helicity spectrum  $\rho_b(k) = H_b(k)/(\langle |\mathbf{a}_k|^2 \rangle^{1/2} \langle |\mathbf{b}_k|^2 \rangle^{1/2})$  in order to quantify how far the flow is from a maximally helical state. It is clear that the magnetic field becomes fully helical only at the largest scale of the flow while the rest of the scales have moderate values of  $\rho_b(k)$ .

The magnetic field can also be sustained without forcing the induction equation, i.e., by dynamo action. A recent numerical investigation [21] of the kinematic dynamo with  $k_f L \gg 1$  found that at scales larger than the forcing scale the kinetic energy scales as  $k^2$ , in agreement with our results, while the magnetic energy scales as  $k^0$ . We expect that the scaling of the magnetic energy will change in the nonlinear stage of the dynamo, where the Lorentz force is nonnegligible, and we speculate that a  $k^2$  spectrum will form in the saturated regime of the dynamo. However, this is something that has to be confirmed.

In this paper, we investigated the dynamics of magnetic helicity focusing on the large scales of MHD turbulence. We demonstrate that the inverse cascade of magnetic helicity at steady state occurs nonlocally from the energy injection scale into the largest scales of the flows we considered. By increasing scale separation, we observe that the inverse energy transfer diminishes and hence no magnetic helicity and almost no total energy is transferred to an intermediate range of scales larger than the forcing length scale but also sufficiently smaller than the box size. Therefore, we show that in this range of scales, helical MHD turbulence is described to a large extent by the (zero flux) absolute equilibrium spectra, with deviations expected at scales close to the largest available scale of the system. Our results have direct implications for the understanding of the preservation of planetary and stellar magnetic fields on scales much larger than the size of these astrophysical objects.

Acknowledgements: We thank A. Berera for access to HPC resources and M. McKay for technical help. This work has made use of the resources provided by ARCHER [22], made available through the Edinburgh Compute and Data Facility (ECDF)[23]. V. D. acknowledges support from the Royal Society and the British Academy of Sciences (Newton International Fellowship, Grant No. NF140631). M. L. acknowledges support from the UK Engineering and Physical Sciences Research Council (EP/K503034/1). The research leading to these results has received funding from the European Union's Seventh Framework Programme (FP7/2007-2013) under Grant Agreement No. 339032.

[1] H. K. Moffatt, *Magnetic Field Generation in Electrically Conducting Fluids* (Cambridge University Press, Cambridge, 1978).  
 [2] U. Frisch, A. Pouquet, J. Léorat, and A. Mazure, J.

Fluid Mech. **68**, 769 (1975).  
 [3] A. Brandenburg and K. Subramanian, Phys. Rep. **417**, 1 (2005).  
 [4] A. Brandenburg, Astrophys. Journal **550**, 824 (2001).

- [5] A. Alexakis, P. D. Mininni, and A. Pouquet, *Astrophys. J.* **640**, 335 (2006).
- [6] W. C. Müller, S. K. Malapaka, and A. Busse, *Phys. Rev. E* **85**, 015302 (2012).
- [7] P. D. Mininni, *Annu. Rev. Fluid Mech.* **43**, 377 (2011).
- [8] O. Debliquy, M. K. Verma, and D. Carati, *Phys. Plasmas* **12**, 042309 (2005).
- [9] A. Alexakis, P. D. Mininni, and A. Pouquet, *Phys. Rev. E* **72**, 046301 (2005).
- [10] M. F. Linkmann, A. Berera, M. E. McKay and J. Jäger, *J. Fluid Mech.* **791**, 61 (2016).
- [11] V. Dallas and A. Alexakis, *Physics of Fluids* **27**, 045105 (2015).
- [12] S. K. Malapaka and W.-C. Müller, *Astrophys. J.* **778**, 21 (2013).
- [13] E. A. Novikov, *Soviet Phys. JETP* **20**, 1290 (1965).
- [14] S. R. Yoffe, Ph.D. thesis, University of Edinburgh.
- [15] A. Berera and M. F. Linkmann, *Phys. Rev. E* **90**, 041003(R) (2014).
- [16] V. Borue and S. A. Orszag, *Phys. Rev. E* **51**, 856(R) (1995).
- [17] A. G. Lamorgese, D. A. Caughey, and S. B. Pope, *Physics of Fluids* **17**, 015106 (2005).
- [18] U. Frisch, *Turbulence: The Legacy of A. N. Kolmogorov* (Cambridge University Press, Cambridge, 1995).
- [19] P. A. Davidson, *Turbulence: An Introduction for scientists and engineers* (Oxford University Press, Oxford, 2004).
- [20] V. Dallas, S. Fauve, and A. Alexakis, *Phys. Rev. Lett* **115**, 204501 (2015).
- [21] M. Sadek, A. Alexakis, and S. Fauve, *Phys. Rev. Lett.* **116**, 074501 (2016).
- [22] <http://www.archer.ac.uk/>.
- [23] <http://www.ecdf.ed.ac.uk/>.